

The Influence of Temperature on Ozone Production under varying NO_x Conditions – a modelling study

J. Coates¹, K. Mar¹, N. Ojha² and T. Butler¹

¹Institute for Advanced Sustainability Studies, Potsdam, Germany

²Atmospheric Chemistry Department, Max Planck Institute for Chemistry, Mainz,
Germany

March 24, 2016

Abstract

Surface ozone is a secondary air pollutant produced during the atmospheric photochemical degradation of emitted volatile organic compounds (VOCs) in the presence of sunlight and nitrogen oxides (NO_x). Temperature directly influences ozone production through speeding up the rates of the chemical reactions and increasing the emissions of VOCs, such as isoprene, from vegetation. In this study, we used a box model to examine the non-linear relationship between ozone, NO_x and temperature, and compared this to previous observational studies. Under high-NO_x conditions, an increase in ozone from 20 °C to 40 °C of up to 20 ppbv was due to faster reaction rates while increased isoprene emissions added up to a further 11 ppbv of ozone. The increased oxidation rate of emitted VOC with temperature controlled the rate of O_x production, the net influence of peroxy nitrates increased net O_x production per molecule of emitted VOC oxidised. The rate of increase in ozone mixing ratios with temperature from our box model simulations was about half the rate of increase in ozone with temperature observed over central Europe or simulated by a regional chemistry transport model. Modifying the box model setup to approximate stagnant meteorological conditions increased the rate of increase of ozone with temperature as the accumulation of oxidants enhanced ozone production through the increased production of peroxy radicals from the secondary degradation of emitted VOCs. The box model simulations approximating stagnant conditions and the maximal ozone production chemical regime reproduced the 2 ppbv increase in ozone per °C from the observational and regional model data over central Europe. The simulated ozone-temperature relationship was more sensitive to mixing than the choice of

chemical mechanism. Our analysis suggests that reductions in NO_x emissions would be required to offset the additional ozone production due to an increase in temperature in the future.

1 Introduction

Surface-level ozone (O_3) is a secondary air pollutant formed during the photochemical degradation of volatile organic compounds (VOCs) in the presence of nitrogen oxides ($\text{NO}_x \equiv \text{NO} + \text{NO}_2$). Due to the photochemical nature of ozone production, it is strongly influenced by meteorological variables such as temperature (Jacob and Winner, 2009). Otero et al. (2016) showed that temperature was a major meteorological driver for summertime ozone in many areas of central Europe.

Temperature primarily influences ozone production in two ways: speeding up the rates of many chemical reactions, and increasing emissions of VOCs from biogenic sources (BVOCs) (Sillman and Samson, 1995). While emissions of anthropogenic VOCs (AVOCs) are generally not dependent on temperature, evaporative emissions of some AVOCs do increase with temperature (Rubin et al., 2006). The review of Pusede et al. (2015) provides further details of the temperature-dependent processes impacting ozone production.

Regional modelling studies over the US (Sillman and Samson, 1995; Steiner et al., 2006; Dawson et al., 2007) examined the sensitivity of ozone production during a pollution episode to increased temperatures. These studies noted that increased temperatures (without changing VOC or NO_x -conditions) led to higher ozone levels, often exceeding local air quality guidelines. Sillman and Samson (1995) and Dawson et al. (2007) varied the temperature dependence of the PAN (peroxy acetyl nitrate) decomposition rate during simulations of the eastern US determining the sensitivity of ozone production with temperature to the PAN decomposition rate. In addition to the influence of PAN decomposition on ozone production, Steiner et al. (2006) correlated the increase in ozone mixing ratios with temperature over California to increased mixing ratios of formaldehyde, a secondary degradation product of many VOCs and an important radical source. Steiner et al. (2006) also noted increased emissions of BVOCs at higher temperatures in urban areas with high NO_x emissions also increased ozone levels with temperature.

Pusede et al. (2014) used an analytical model constrained by observations over the San Joaquin Valley, California to infer a non-linear relationship between ozone, temperature and NO_x , similar to the well-known non-linear relationship of ozone production on NO_x and VOC

60 levels (Sillman, 1999). Moreover, Pusede et al. (2014) showed that temperature can be used
61 as a surrogate for VOC levels when considering the relationship of ozone under different NO_x
62 conditions.

63 Environmental chamber studies have also been used to analyse the relationship of ozone with
64 temperature using a fixed mixture of VOCs. The chamber experiments of Carter et al. (1979)
65 and Hatakeyama et al. (1991) showed increases in ozone from a VOC mix with temperature.
66 Both studies compared the concentration time series of ozone and nitrogen-containing compounds
67 (NO_x , PAN, HNO_3) at various temperatures linking the maximum ozone concentration to the
68 decrease in PAN concentrations at temperatures greater than 303 K.

69 Despite many studies considering the ozone-temperature relationship from an observational
70 and chamber study perspective, modelling studies focusing on the detailed chemical processes of
71 the ozone-temperature relationship under different NO_x conditions have not been performed (to
72 our knowledge). The regional modelling studies described previously concentrated on reproducing
73 ozone levels (using a single chemical mechanism) over regions with known meteorology and
74 NO_x conditions then varying the temperature. These modelling studies did not consider the
75 relationship between ozone, NO_x and temperature. The review of Pusede et al. (2015) also
76 highlights a lack of modelling studies looking at the relationship of ozone with temperature under
77 different NO_x conditions.

78 Comparisons of different chemical mechanisms, such as Emmerson and Evans (2009) and
79 Coates and Butler (2015), showed that different representations of tropospheric chemistry
80 influenced ozone production. Neither of these studies examined the ozone-temperature relationship
81 differences between chemical mechanisms. Furthermore, Rasmussen et al. (2013) acknowledged
82 that the modelled ozone-temperature relationship may be sensitive to the choice of chemical
83 mechanism and recommended investigating this sensitivity. Comparing the ozone-temperature
84 relationship predicted by different chemical mechanisms is potentially important for modelling of
85 future air quality due to the expected increase in heatwaves (Karl and Trenberth, 2003).

86 In this study, we use an idealised box model to determine how ozone levels vary with
87 temperature under different NO_x conditions. We determine whether faster chemical reaction
88 rates or increased BVOC emissions have a greater influence on instantaneous ozone production
89 with higher temperature under different NO_x conditions. Furthermore, we compare the
90 ozone-temperature relationship produced by different chemical mechanisms.

2 Methodology

2.1 Model Setup

We used the MECCA box model (Sander et al., 2005) to determine the important gas-phase chemical processes for ozone production under different temperatures and NO_x conditions. The MECCA box model was set up as described in Coates and Butler (2015) and updated to include vertical mixing with the free troposphere using a diurnal cycle for the PBL height. The supplementary material includes further details of these updates.

Simulations were broadly representative of urban conditions in central Europe and were run for daylight hours in one full day. Methane was fixed at 1.7 ppmv throughout the model run, carbon monoxide (CO) and ozone were initialised at 200 ppbv and 40 ppbv and then allowed to evolve freely throughout the simulation. All VOC emissions were held constant until noon simulating a plume of freshly-emitted VOC.

Separate box model simulations were performed by systematically varying the temperature between 288 and 313 K (15–40 °C) in steps of 0.5 K. NO emissions were systematically varied between 5.0×10^9 and 1.5×10^{12} molecules(NO) $\text{cm}^{-2} \text{s}^{-1}$ in steps of 1×10^{10} molecules(NO) $\text{cm}^{-2} \text{s}^{-1}$ at each temperature step. At 20 °C, these NO emissions corresponded to peak NO_x mixing ratios of 0.02 ppbv and 10 ppbv respectively, this range of NO_x mixing ratios covers the NO_x conditions found in pristine and urban conditions (von Schneidemesser et al., 2015).

All simulations were repeated using different chemical mechanisms to investigate whether the relationship between ozone, temperature and NO_x changes using different representations of ozone production chemistry. The reference chemical mechanism was the near-explicit Master Chemical Mechanism, MCMv3.2, (Jenkin et al., 1997, 2003; Saunders et al., 2003; Rickard et al., 2015). The reduced chemical mechanisms in our study were Common Representative Intermediates, CRIv2 (Jenkin et al., 2008), Model for OZone and Related Chemical Tracers, MOZART-4 (Emmons et al., 2010), Regional Acid Deposition Model, RADM2 (Stockwell et al., 1990) and the Carbon Bond Mechanism, CB05 (Yarwood et al., 2005). Coates and Butler (2015) described the implementation of these chemical mechanisms in MECCA. These reduced chemical mechanisms were chosen as they are commonly used by modelling groups in 3D regional and global models (Baklanov et al., 2014).

Model runs were repeated using a temperature-dependent and temperature-independent

Table 1: Total AVOC emissions in 2011 in tonnes from each anthropogenic source category assigned from TNO-MACC_III emission inventory and temperature-independent BVOC emissions in tonnes from Benelux region assigned from EMEP. The allocation of these emissions to MCMv3.2, CRIv2, CB05, MOZART-4 and RADM2 species are found in the supplementary material.

Source Category	Total Emissions	Source Category	Total Emissions
Public Power	13755	Road Transport: Diesel	6727
Residential Combustion	21251	Road Transport: Others	1433
Industry	62648	Road Transport: Evaporation	2327
Fossil Fuel	15542	Non-road Transport	17158
Solvent Use	100826	Waste	1342
Road Transport: Gasoline	24921	BVOC	10702

source of BVOC emissions to determine the relative importance of increased emissions of BVOC and faster reaction rates of chemical processes for the increase of ozone with temperature. MEGAN2.1 (Guenther et al., 2012) specified the temperature-dependent BVOC emissions of isoprene, Sect. 2.3 provides further details. As isoprene emissions are the most important source of BVOC on the global scale (Guenther et al., 2006), we considered only isoprene emissions from vegetation. Only isoprene emissions were dependent on temperature, all other emissions were constant in all simulations. In reality, many other BVOC are emitted from varying vegetation types (Guenther et al., 2006) and increased temperature can also increase AVOC emissions through increased evaporation (Rubin et al., 2006).

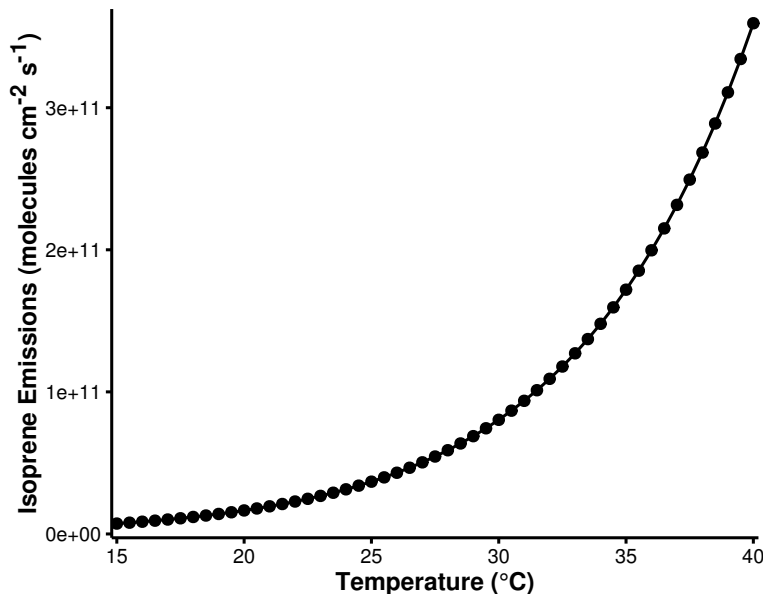
2.2 VOC Emissions

Emissions of urban AVOC over central Europe were taken from the TNO-MACC_III emission inventory for the Benelux (Belgium, Netherlands and Luxembourg) region for the year 2011. TNO-MACC_III is the updated TNO-MACC_II emission inventory created using the same methodology as Kuenen et al. (2014) and based upon improvements to the existing emission inventory during AQMEII-2 (Pouliot et al., 2015).

Temperature-independent emissions of isoprene and monoterpenes from biogenic sources were calculated as a fraction of the total AVOC emissions from each country in the Benelux region. This data was obtained from the supplementary data available from the EMEP (European Monitoring and Evaluation Programme) model (Simpson et al., 2012). Temperature-dependent emissions of isoprene are described in Sect. 2.3.

Table 1 shows the quantity of VOC emissions from each source category and the

Figure 1: The estimated isoprene emissions (molecules isoprene $\text{cm}^{-2} \text{s}^{-1}$) using MEGAN2.1 at each temperature used in the study.



temperature-independent BVOC emissions. These AVOC emissions were assigned to chemical species and groups based on the profiles provided by TNO. The NMVOC emissions were speciated to MCMv3.2 species as described by von Schneidmesser et al. (2016). For simulations done with other chemical mechanisms, the VOC emissions represented by the MCMv3.2 were mapped to the mechanism species representing VOC emissions in each reduced chemical mechanism based on the recommendations of the source literature and Carter (2015). The VOC emissions in the reduced chemical mechanisms were weighted by the carbon numbers of the MCMv3.2 species and the emitted mechanism species, thus keeping the amount of emitted reactive carbon constant between simulations. The supplementary data outlines the primary VOC and calculated emissions with each chemical mechanism.

2.3 Temperature Dependent Isoprene Emissions

Temperature-dependent emissions of isoprene were estimated using the MEGAN2.1 algorithm for calculating the emissions of VOC from vegetation (Guenther et al., 2012). Emissions from nature are dependent on many variables including temperature, radiation and age of vegetation but for the purpose of our study all variables except temperature were held constant.

The MEGAN2.1 parameters were chosen to give similar isoprene mixing ratios at 20 °C to the temperature-independent emissions of isoprene in order to compare the effects of increased isoprene emissions with temperature. The estimated emissions of isoprene with MEGAN2.1

Table 2: Increase in mean ozone mixing ratio (ppbv) due to chemistry (i.e. faster reaction rates) and temperature-dependent isoprene emissions from 20 °C to 40 °C in the NO_x-regimes of Fig. 3.

Chemical Mechanism	Source of Difference	Increase in Ozone from 20 °C to 40 °C (ppbv)		
		Low-NO _x	Maximal-O ₃	High-NO _x
MCMv3.2	Isoprene Emissions Chemistry	4.6	7.7	10.6
		6.8	12.5	15.2
CRIV2	Isoprene Emissions Chemistry	4.8	7.9	10.8
		6.0	11.1	13.7
MOZART-4	Isoprene Emissions Chemistry	4.1	6.7	10.0
		6.0	10.2	12.3
CB05	Isoprene Emissions Chemistry	4.6	7.4	9.8
		9.3	16.0	19.9
RADM2	Isoprene Emissions Chemistry	3.8	5.7	7.8
		8.6	14.1	17.3

using these assumptions are illustrated in Fig. 1 and show the expected exponential increase in isoprene emissions with temperature (Guenther et al., 2006).

The estimated emissions of isoprene at 20 °C lead to 0.07 ppbv of isoprene in our simulations while at 30 °C, the increased emissions of isoprene using MEGAN2.1 estimations lead to 0.35 ppbv of isoprene in the model. A measurement campaign over Essen, Germany (Wagner and Kuttler, 2014) measured 0.1 ppbv of isoprene at temperature 20 °C and 0.3 ppbv of isoprene were measured at 30 °C. The similarity of the simulated and observed isoprene mixing ratios indicates that the MEGAN2.1 variables chosen for calculating the temperature-dependent emissions of isoprene were suitable for simulating urban conditions over central Europe.

3 Results and Discussion

3.1 Relationship between Ozone, NO_x and Temperature

Figure 2 depicts the peak mixing ratio from ozone of each simulation as a function of the total NO_x emissions and temperature when using a temperature-independent and temperature-dependent source of isoprene emissions for each chemical mechanism. A non-linear relationship of ozone mixing ratios with NO_x and temperature is produced by each chemical mechanism. This non-linear relationship is similar to that determined by Pusede et al. (2014) using an analytical model constrained to observational measurements over the San Joaquin Valley, California.

Higher peak ozone mixing ratios are produced when using a temperature-dependent source of isoprene emissions (Fig. 2). The highest mixing ratios of peak ozone are produced at high temperatures and moderate emissions of NO_x regardless of the temperature dependence of isoprene emissions. Conversely, the least amount of peak ozone is produced with low emissions of

Figure 2: Contours of peak ozone mixing ratios (ppbv) as a function of the total NO_x emissions and temperature for each chemical mechanism using a temperature-dependent and temperature-independent source of isoprene emissions. The contours can be split into three separate regimes: High- NO_x , Maximal- O_3 and Low- NO_x indicated in the figure.

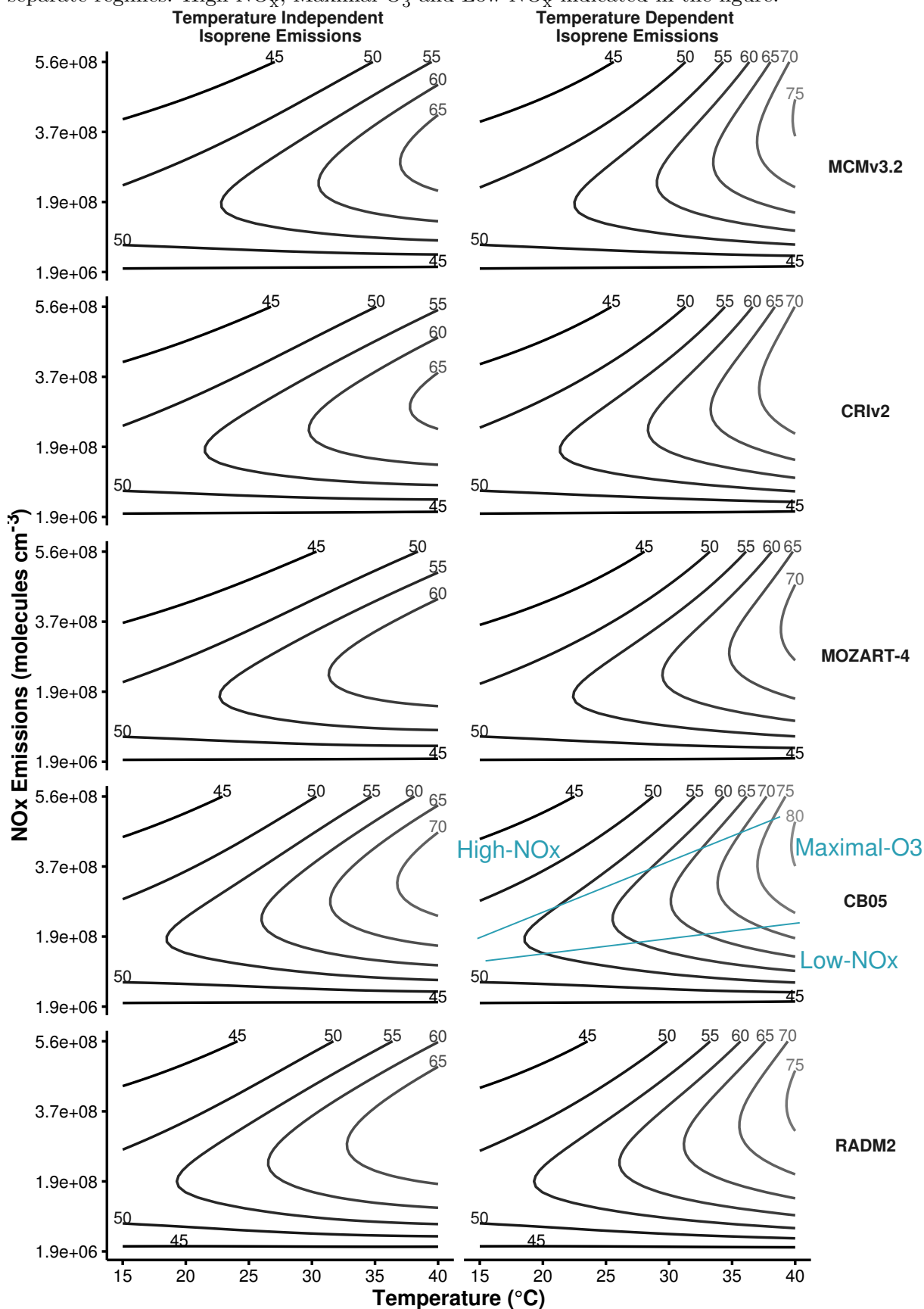
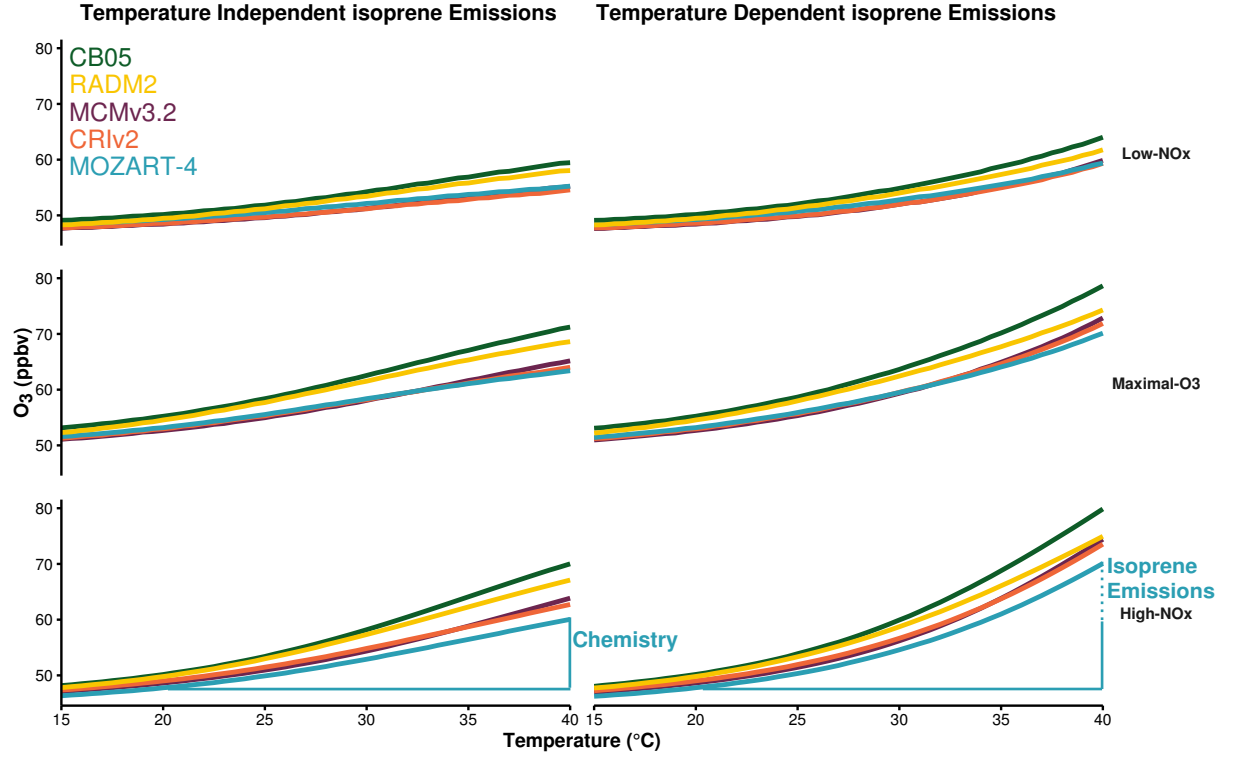


Figure 3: Mean ozone mixing ratios (ppbv) at each temperature after allocation to the different NO_x -regimes of Fig. 2. The differences in ozone mixing ratios due to chemistry (solid line) and isoprene emissions (dotted line) are represented graphically for MOZART-4 with High- NO_x conditions. Table 2 details the differences for each chemical mechanism and NO_x -condition.



NO_x over the whole temperature range (15 – 40 °C) when using both a temperature-independent and temperature-dependent source of isoprene emissions.

The contours of ozone mixing ratios as a function of NO_x and temperature can be split into three NO_x regimes (Low- NO_x , Maximal- O_3 and High- NO_x), similar to the NO_x regimes defined for the non-linear relationship of ozone with VOC and NO_x . The Low- NO_x regime corresponds with regions having little increase in ozone with temperature, also called the NO_x -sensitive regime. The High- NO_x (or NO_x -saturated) regime is when ozone levels increase rapidly with temperature. The contour ridges correspond to regions of maximal ozone production; this is the Maximal- O_3 regime. Pusede et al. (2014) showed that temperature can be used as a proxy for VOC, thus we assigned the ozone mixing ratios from each box model simulation to a NO_x regime based on the $\text{H}_2\text{O}_2:\text{HNO}_3$ ratio. This ratio was used by Sillman (1995) to designate ozone to NO_x regimes based on NO_x and VOC levels. The Low- NO_x regime corresponds to $\text{H}_2\text{O}_2:\text{HNO}_3$ ratios less than 0.5, the High- NO_x regime corresponds to ratios larger than 0.3 and ratios between 0.3 and 0.5 correspond to the Maximal- O_3 regime.

The peak ozone mixing ratio from each simulation was assigned to a NO_x regime based on the $\text{H}_2\text{O}_2:\text{HNO}_3$ ratio of that simulation. The peak ozone mixing ratios assigned to each NO_x regime

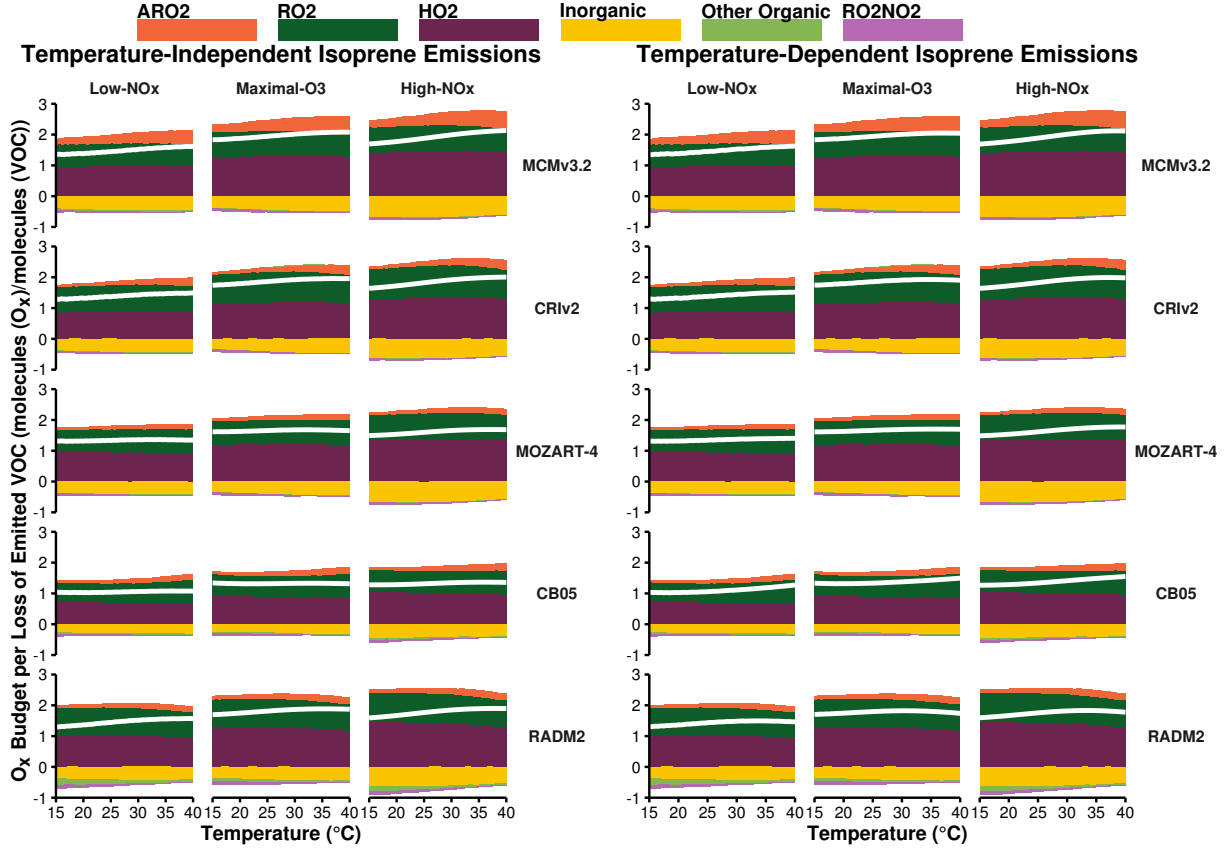
at each temperature were averaged, and illustrated in Fig. 3 for each chemical mechanism and each type of isoprene emissions (temperature independent and temperature dependent). We define the absolute increase in ozone from 20 °C to 40 °C due to faster reaction rates as the difference between ozone mixing ratios from 20 °C to 40 °C when using a temperature-independent source of isoprene emissions. When using a temperature-dependent source of isoprene emissions, the difference in ozone mixing ratios from 20 °C to 40 °C minus the increase due to faster reaction rates, gives the absolute increase in ozone mixing ratios from increased isoprene emissions. These differences are represented graphically in Fig. 3 and summarised in Table 2.

Table 2 shows that the absolute increase in ozone with temperature due to chemistry (i.e. faster reaction rates) is larger than the absolute increase in ozone due to increased isoprene emissions for each chemical mechanism and each NO_x regime. In all cases the absolute increase in ozone with temperature is largest under High- NO_x conditions and lowest with Low- NO_x conditions (Fig. 3 and Table 2). The increase in ozone mixing ratio from 20 °C to 40 °C due to faster reaction rates with High- NO_x conditions is almost double that with Low- NO_x conditions. In the Low- NO_x regime, the increase of ozone with temperature using the reduced chemical mechanisms (CRIV2, MOZART-4, CB05 and RADM2) is similar to that from the MCMv3.2. Larger differences occur in the Maximal- O_3 and High- NO_x regimes.

All reduced chemical mechanisms except RADM2 have similar increases in ozone due to increased isoprene emissions as the MCMv3.2 (Table 2). RADM2 produces 3 ppbv less ozone than the MCMv3.2 due to increased isoprene emissions in each NO_x regime, indicating that this difference is due the representation of isoprene degradation chemistry in RADM2.

Coates and Butler (2015) compared ozone production in different chemical mechanisms to the MCMv3.2 using the TOPP metric (Tagged Ozone Production Potential) as defined in Butler et al. (2011) and showed that less ozone is produced per molecule of isoprene emitted using RADM2 than with MCMv3.2. The degradation of isoprene has been extensively studied and it is well-known that methyl vinyl ketone (MVK) and methacrolein are signatures of isoprene degradation (Atkinson, 2000). All chemical mechanisms in our study except RADM2 explicitly represent MVK and methacrolein (or in the case of CB05, a lumped species representing both these secondary degradation products). RADM2 does not represent methacrolein and the mechanism species representing ketones (KET) is a mixture of acetone and methyl ethyl ketone (MEK) (Stockwell et al., 1990). Thus the secondary degradation of isoprene in RADM2 is unable to represent the ozone production from the further degradation of the signature secondary

Figure 4: Day-time budgets of O_x normalised by the total loss rate of emitted VOC in the NO_x -regimes of Fig. 3. The white line indicates net production or consumption of O_x . The net contribution of reactions to O_x budgets are allocated to categories of inorganic reactions, peroxy nitrates (RO2NO2), reactions of NO with HO2, alkyl peroxy radicals (RO2) and acyl peroxy radicals (ARO2). All other reactions are allocated to the ‘Other Organic’ category.



degradation products of isoprene, MVK and methacrolein. Updated versions of RADM2, RACM
 (Stockwell et al., 1997) and RACM2 (Goliff et al., 2013), sequentially included methacrolein and
 MVK and with these updates the ozone production from isoprene oxidation approached that of
 the MCMv3.2 (Coates and Butler, 2015).

3.2 Ozone Production and Consumption Budgets

In order to understand the temperature dependence of ozone production directly, we examine
 the modelled day-time production and consumption budgets of O_x ($\equiv O_3 + NO_2 + O(^1D) + O$)
 normalised by the total chemical loss rate of the emitted VOC (Fig. 4). The O_x budgets are
 assigned to each NO_x regime for each chemical mechanism and type of isoprene emissions. The
 budgets are allocated to the net contribution of major chemical categories, where ‘HO2’, ‘RO2’,
 ‘ARO2’ represent the reactions of NO with HO_2 , alkyl peroxy radicals and acyl peroxy radicals
 respectively. ‘RO2NO2’ represents the net effects of peroxy nitrates, which remove O_x when
 produced and are a source of O_x when they thermally decompose. ‘Inorganic’ is all other inorganic

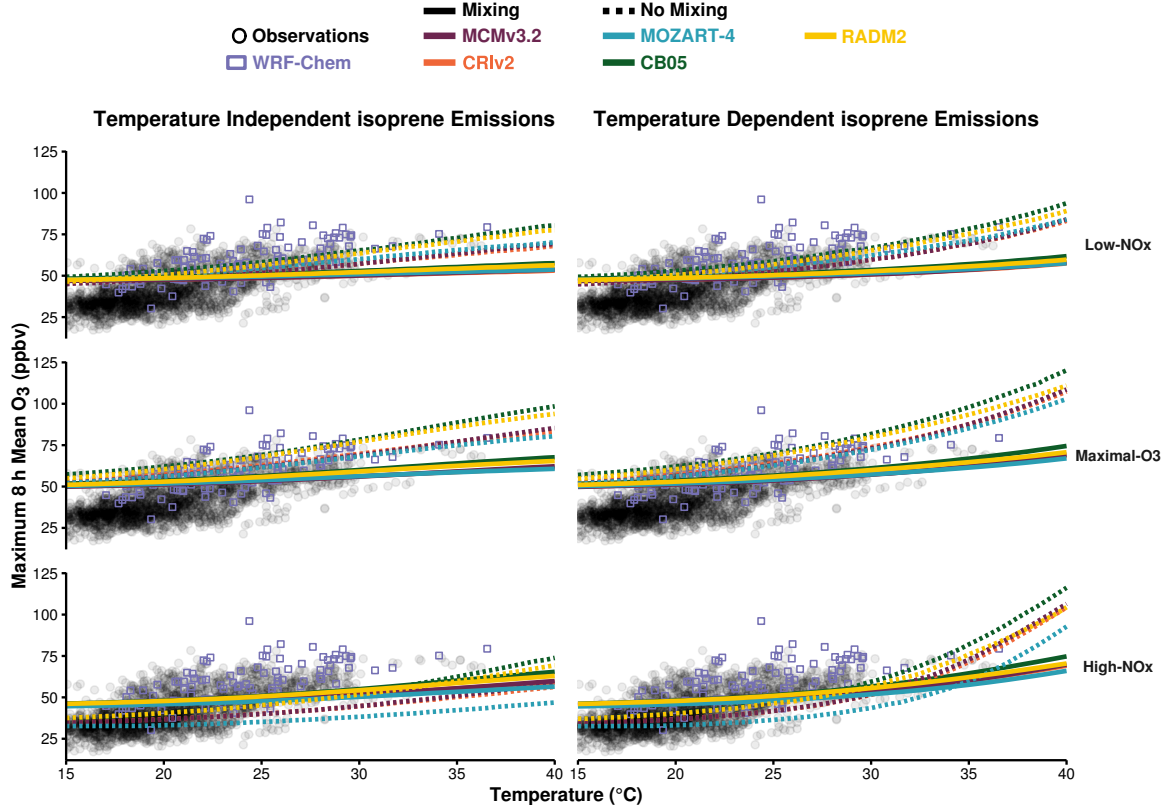
contributions to O_x production and any other remaining organic reactions are included in the ‘Other Organic’ category. Figure 4 also illustrates the net production or consumption of O_x in each case. The ratio of net ozone to net O_x production was practically constant with temperature in all cases showing that using O_x budgets as a proxy for ozone budgets was suitable at each temperature in our study. The absolute production and consumption budgets of O_x allocated to the same source categories as Fig. 4 are included in the supplementary material and further illustrate the increase in O_x production with temperature.

The net O_x production efficiency increases from 20 °C to 40 °C by ~ 0.25 molecules of O_x per molecule of VOC oxidised with each NO_x -condition and type of isoprene emissions using the detailed MCMv3.2 chemical mechanism (Fig. 4). A lower increase in normalised net O_x production efficiency from 20 °C to 40 °C was obtained with the reduced chemical mechanisms (~ 0.2 molecules of O_x per molecule of VOC oxidised with CRIv2, CB05 and RADM2, and ~ 0.1 molecules of O_x per molecule of VOC oxidised using MOZART-4). The increase in net O_x production efficiency is due to the increased contribution with temperature of acyl peroxy radicals (ARO2) reacting with NO and the decreased net contribution with temperature of RO2NO2 (peroxy nitrates) to the normalised O_x budgets.

The increased contribution of ARO2 to O_x production with temperature is linked to the decreased net contribution of RO2NO2 with temperature to O_x budgets as peroxy nitrates are produced from the reactions of acyl peroxy radicals with NO_2 . The decomposition rate of peroxy nitrates is strongly temperature dependent and at higher temperatures the faster decomposition rate of RO2NO2 leads to faster release of acyl peroxy radicals and NO_2 . Thus the equilibrium of RO2NO2 shifts towards thermal decomposition with increasing temperature leading to the increased contribution of ARO2 with temperature to O_x production (Fig. 4). Dawson et al. (2007) attributed the increase in maximum 8 h ozone mixing ratios with temperature during a modelling study over the eastern US to the decrease in PAN lifetime with temperature. Steiner et al. (2006) also recognised that the decrease in PAN lifetime with temperature contributed to the increase of ozone with temperature concluding that the combined effects of increased oxidation rates of VOC and faster PAN decomposition increased the production of ozone with temperature.

As the production efficiency of O_x remains constant with temperature (~ 2 molecules of O_x per molecule of VOC oxidised, Fig. 4), the rate of O_x production is controlled by the oxidation of VOCs. Faster oxidation of VOCs with temperature speeds up the production of peroxy radicals

Figure 5: MDA8 values of ozone from the box model simulations allocated to the different NO_x regimes for each chemical mechanism with mixing (solid lines) and without mixing (dashed lines). The box model ozone-temperature correlation is compared to the summer 2007 observational data (black circles) and WRF-Chem output (purple boxes).



increasing ozone production when peroxy radicals react with NO to produce NO_2 . The reactivity of VOCs has been linked to ozone production (e.g. Kleinman (2005), Sadanaga et al. (2005)) and the review of Pusede et al. (2015) acknowledged the importance of organic reactivity and radical production to the ozone-temperature relationship. Also, the modelling study of Steiner et al. (2006) noted that the increase in initial oxidation rates of VOCs with temperature leads to increased formaldehyde concentrations and in turn an increase of ozone as formaldehyde is an important source of HO_2 radicals.

3.3 Comparison to Observations and 3D Model Simulations

This section compares the results from our idealised box model simulations to real-world observations and model output from a 3D model. Using the interpolated observations of the maximum daily 8 h mean (MDA8) of ozone from Schnell et al. (2015) and the meteorological observational data set of the ERA-Interim re-analysis, Otero et al. (2016) showed that over the summer (JJA) months, temperature is the main meteorological driver of ozone production over many regions of central Europe. Model output from the 3D WRF-Chem regional model using

Table 3: Slopes (m_{O_3-T} , ppbv per $^{\circ}C$) of the linear fit to MDA8 values of ozone and temperature correlations in Fig. 5, indicating the increase of MDA8 in ppbv of ozone per $^{\circ}C$. The slope of the observational data is 2.15 ppbv/ $^{\circ}C$ and the slope of the WRF-Chem output is 2.05 ppbv/ $^{\circ}C$.

Mechanism	Isoprene Emissions	Low- NO_x		Maximal- O_3		High- NO_x	
		Mixing	No Mixing	Mixing	No Mixing	Mixing	No Mixing
MCMv3.2	Temperature Independent	0.28	1.01	0.51	1.36	0.59	0.96
	Temperature Dependent	0.42	1.48	0.74	2.16	0.93	2.63
CRIV2	Temperature Independent	0.25	0.93	0.47	1.27	0.55	0.88
	Temperature Dependent	0.40	1.44	0.71	2.09	0.90	2.52
MOZART-4	Temperature Independent	0.25	0.97	0.44	1.21	0.49	0.59
	Temperature Dependent	0.38	1.43	0.65	1.98	0.81	2.05
CB05	Temperature Independent	0.39	1.30	0.67	1.72	0.79	1.45
	Temperature Dependent	0.52	1.72	0.89	2.44	1.12	2.94
RADM2	Temperature Independent	0.37	1.31	0.61	1.64	0.70	1.28
	Temperature Dependent	0.48	1.68	0.79	2.22	0.97	2.49

MOZART-4 chemistry set-up over the European domain for simulations of the year 2007 from Mar et al. (2016) was used to further compare the box model simulations to a model including more meteorological processes than our box model.

Figure 5 compares the observational and WRF-Chem data from summer 2007 averaged over central and eastern Germany, where summertime ozone values are driven by temperature (Otero et al., 2016), to the MDA8 values of ozone from the box model simulations for each chemical mechanism (solid lines). Despite a high bias in simulated ozone in WRF-Chem, the rate of change of ozone with temperature from the WRF-Chem simulations (2.05 ppbv/ $^{\circ}C$) is similar to the rate of change of ozone with temperature from the observed data (2.15 ppbv/ $^{\circ}C$). The differences in ozone production between the different chemical mechanisms with the box model are small compared to the spread of the observational and WRF-Chem data. A temperature-dependent source of isoprene with high- NO_x conditions produces the highest ozone-temperature slope, but is still lower than the observed ozone-temperature slope by a factor of two. In particular, the box model simulations over-predict the ozone values at lower temperatures and under-predict the ozone values at higher temperatures compared to the observed data.

In our simulations, we focused on instantaneous production of ozone from a freshly-emitted source of VOC with mixing of clean air from the free troposphere due to a growing boundary layer. This box model setup did not consider stagnant atmospheric conditions characterized by low wind speeds slowing the transport of ozone and its precursors away from sources. Stagnant conditions have been correlated to high-ozone episodes in the summer over eastern US (Jacob et al., 1993).

In order to investigate the sensitivity of ozone production to mixing, box model simulations

were performed without vertical mixing to approximate stagnant conditions that favour accumulation of secondary VOC oxidation products. The ozone-temperature relationship obtained with each chemical mechanism, using both a temperature-independent and temperature-dependent source of isoprene emissions and the different NO_x conditions are displayed in Fig. 5 (dotted lines). Table 3 summarises the slopes ($m_{\text{O}_3\text{-T}}$) of the linear fits of the box model simulations displayed in Fig. 5 in ppbv of ozone per $^\circ\text{C}$ determining the rate of increase of ozone with temperature, for both case: with, and without mixing.

For all chemical mechanisms, the rate of increase of ozone with temperature increased in the box model simulations without mixing. The $m_{\text{O}_3\text{-T}}$ calculated from the box model simulations without mixing using a temperature-dependent source of isoprene and with Maximal- O_3 conditions (ranging between 2.0 and 2.4 ppbv/ $^\circ\text{C}$) are very similar to the slopes of the observational and WRF-Chem results (2.1 and 2.2 ppbv/ $^\circ\text{C}$, respectively). The differences in $m_{\text{O}_3\text{-T}}$ when not including mixing in the box model compared to the differences in $m_{\text{O}_3\text{-T}}$ between chemical mechanisms in Table 3 show that the ozone-temperature relationship using our box model setup is more sensitive to mixing than the choice of chemical mechanism.

An analysis similar to that presented in Fig. 4 shows no appreciable difference between the cases with and without mixing (not shown). The chemical production of O_x in each chemical mechanism normalised by the chemical loss rate of VOC remains unchanged. Furthermore, the supplementary material includes the absolute production and consumption budgets of O_x which also show the increased O_x production with temperature for the simulations performed without mixing. From this we conclude that the increased ozone production seen in the box model simulations with reduced mixing is due to enhanced OH reactivity from secondary VOC oxidation products.

4 Conclusions

In this study, we determined the effects of temperature on ozone production using a box model over a range of temperatures and NO_x conditions with a temperature-independent and temperature-dependent source of isoprene emissions. These simulations were repeated using reduced chemical mechanism schemes (CRIV2, MOZART-4, CB05 and RADM2) typically used in 3D models and compared to the near-explicit MCMv3.2 chemical mechanism.

Each chemical mechanism produced a non-linear relationship of ozone with temperature

and NO_x with the most ozone produced at high temperatures and moderate emissions of NO_x . Conversely, lower NO_x levels led to a minimal increase of ozone with temperature. Thus air quality in a future with higher temperatures would benefit from reductions in NO_x emissions.

Faster reaction rates at higher temperatures were responsible for a greater absolute increase in ozone than increased isoprene emissions. In our simulations, ozone production was controlled by the increased rate of VOC oxidation with temperature. The net influence of peroxy nitrates increased the net production of O_x per molecule of emitted VOC oxidised with temperature.

The rate of increase of ozone with temperature using observational data over Europe was twice as high as the rate of increase of ozone with temperature when using the box model. This was consistent with our box model setup not representing stagnant atmospheric conditions that are inherently included in observational data and models including meteorology, such as WRF-Chem. In model simulations without mixing the rate of increase of ozone with temperature was faster than the simulations including mixing. The simulations without mixing and a maximal ozone production chemical regime led to very similar rates of increase of ozone with temperature to the observational and WRF-Chem data. Furthermore, the ozone-temperature relationship was more sensitive to mixing than the choice of chemical mechanism.

Acknowledgements

The authors would like to thank Noelia Otero Felipe for providing the ERA-Interim data.

References

- R. Atkinson. Atmospheric chemistry of VOCs and NO_x . *Atmospheric Environment*, 34(12-14): 2063–2101, 2000.
- A. Baklanov, K. Schlünzen, P. Suppan, J. Baldasano, D. Brunner, S. Aksoyoglu, G. Carmichael, J. Douros, J. Flemming, R. Forkel, S. Galmarini, M. Gauss, G. Grell, M. Hirtl, S. Joffre, O. Jorba, E. Kaas, M. Kaasik, G. Kallos, X. Kong, U. Korsholm, A. Kurganskiy, J. Kushta, U. Lohmann, A. Mahura, A. Manders-Groot, A. Maurizi, N. Moussiopoulos, S. T. Rao, N. Savage, C. Seigneur, R. S. Sokhi, E. Solazzo, S. Solomos, B. Sørensen, G. Tsegas, E. Vignati, B. Vogel, and Y. Zhang. Online coupled regional meteorology chemistry models in Europe: current status and prospects. *Atmospheric Chemistry and Physics*, 14(1):317–398, 2014.

369 T. Butler, M. Lawrence, D. Taraborrelli, and J. Lelieveld. Multi-day ozone production potential
 370 of volatile organic compounds calculated with a tagging approach. *Atmospheric Environment*, 45
 371 (24):4082 – 4090, 2011.

372 W. P. L. Carter. Development of a Database for Chemical Mechanism Assignments for Volatile
 373 Organic Emissions. *Journal of the Air & Waste Management Association*, 0, 2015.

374 W. P. L. Carter, A. M. Winer, K. R. Darnall, and J. N. P. Jr. Smog chamber studies of temperature
 375 effects in photochemical smog. *Environmental Science & Technology*, 13(9):1094–1100, 1979.

376 J. Coates and T. M. Butler. A comparison of chemical mechanisms using tagged ozone production
 377 potential (TOPP) analysis. *Atmospheric Chemistry and Physics*, 15(15):8795–8808, 2015.

378 J. P. Dawson, P. J. Adams, and S. N. Pandis. Sensitivity of ozone to summertime climate in the
 379 eastern USA: A modeling case study . *Atmospheric Environment*, 41(7):1494 – 1511, 2007.

380 K. M. Emmerson and M. J. Evans. Comparison of tropospheric gas-phase chemistry schemes for
 381 use within global models. *Atmospheric Chemistry and Physics*, 9(5):1831–1845, 2009.

382 L. K. Emmons, S. Walters, P. G. Hess, J.-F. Lamarque, G. G. Pfister, D. Fillmore, C. Granier,
 383 A. Guenther, D. Kinnison, T. Laepple, J. Orlando, X. Tie, G. Tyndall, C. Wiedinmyer, S. L.
 384 Baughcum, and S. Kloster. Description and evaluation of the Model for Ozone and Related
 385 chemical Tracers, version 4 (MOZART-4). *Geoscientific Model Development*, 3(1):43–67, 2010.

386 W. S. Goliff, W. R. Stockwell, and C. V. Lawson. The regional atmospheric chemistry mechanism,
 387 version 2. *Atmospheric Environment*, 68:174 – 185, 2013.

388 A. Guenther, T. Karl, P. Harley, C. Wiedinmyer, P. I. Palmer, and C. Geron. Estimates of global
 389 terrestrial isoprene emissions using MEGAN (Model of Emissions of Gases and Aerosols from
 390 Nature). *Atmospheric Chemistry and Physics*, 6(11):3181–3210, 2006.

391 A. B. Guenther, X. Jiang, C. L. Heald, T. Sakulyanontvittaya, T. Duhl, L. K. Emmons, and
 392 X. Wang. The Model of Emissions of Gases and Aerosols from Nature version 2.1 (MEGAN2.1):
 393 an extended and updated framework for modeling biogenic emissions. *Geoscientific Model
 394 Development*, 5(6):1471–1492, 2012.

395 S. Hatakeyama, H. Akimoto, and N. Washida. Effect of temperature on the formation of
 396 photochemical ozone in a propene-nitrogen oxide (NO_x)-air-irradiation system. *Environmental
 397 Science & Technology*, 25(11):1884–1890, 1991.

398 D. J. Jacob and D. A. Winner. Effect of climate change on air quality. *Atmospheric Environment*,
399 43(1):51 – 63, 2009. Atmospheric Environment - Fifty Years of Endeavour.

400 D. J. Jacob, J. A. Logan, G. M. Gardner, R. M. Yevich, C. M. Spivakovsky, S. C. Wofsy,
401 S. Sillman, and M. J. Prather. Factors regulating ozone over the United States and its export to
402 the global atmosphere. *Journal of Geophysical Research*, 98(D8), 1993.

403 M. Jenkin, L. Watson, S. Utembe, and D. Shallcross. A Common Representative Intermediates
404 (CRI) mechanism for VOC degradation. Part 1: Gas phase mechanism development. *Atmospheric*
405 *Environment*, 42(31):7185 – 7195, 2008.

406 M. E. Jenkin, S. M. Saunders, and M. J. Pilling. The tropospheric degradation of volatile organic
407 compounds: a protocol for mechanism development. *Atmospheric Environment*, 31(1):81 – 104,
408 1997.

409 M. E. Jenkin, S. M. Saunders, V. Wagner, and M. J. Pilling. Protocol for the development of the
410 Master Chemical Mechanism, MCM v3 (Part B): tropospheric degradation of aromatic volatile
411 organic compounds. *Atmospheric Chemistry and Physics*, 3(1):181–193, 2003.

412 T. R. Karl and K. E. Trenberth. Modern global climate change. *Science*, 302(5651):1719–1723,
413 2003.

414 L. I. Kleinman. The dependence of tropospheric ozone production rate on ozone precursors.
415 *Atmospheric Environment*, 39(3):575 – 586, 2005.

416 J. J. P. Kuenen, A. J. H. Visschedijk, M. Jozwicka, and H. A. C. Denier van der Gon.
417 TNO-MACC_II emission inventory; a multi-year (2003–2009) consistent high-resolution european
418 emission inventory for air quality modelling. *Atmospheric Chemistry and Physics*, 14(20):
419 10963–10976, 2014.

420 K. A. Mar, N. Ojha, A. Pozzer, and T. M. Butler. WRF-Chem Simulations over Europe: Model
421 Evaluation and Chemical Mechanism Comparison. *In Preparation*, 2016.

422 R. Mészáros, I. G. Zsély, D. Szinyei, C. Vincze, and I. Lagzi. Sensitivity analysis of an ozone
423 deposition model. *Atmospheric Environment*, 43(3):663 – 672, 2009.

424 N. Otero, J. Sillmann, J. L. Schnell, H. W. Rust, and T. Butler. Synoptic and meteorological
425 drivers of extreme ozone concentrations over europe. *Environmental Research Letters*, 11(2):
426 024005, 2016.

427 N. Passant. Speciation of UK emissions of non-methane volatile organic compounds. Technical
 428 report, DEFRA, Oxon, UK., 2002.

429 G. Pouliot, H. A. D. van der Gon, J. Kuenen, J. Zhang, M. D. Moran, and P. A. Makar. Analysis
 430 of the emission inventories and model-ready emission datasets of Europe and North America for
 431 phase 2 of the AQMEII project. *Atmospheric Environment*, 115:345–360, 2015.

432 S. E. Pusede, D. R. Gentner, P. J. Wooldridge, E. C. Browne, A. W. Rollins, K.-E. Min, A. R.
 433 Russell, J. Thomas, L. Zhang, W. H. Brune, S. B. Henry, J. P. DiGangi, F. N. Keutsch, S. A.
 434 Harrold, J. A. Thornton, M. R. Beaver, J. M. St. Clair, P. O. Wennberg, J. Sanders, X. Ren,
 435 T. C. VandenBoer, M. Z. Markovic, A. Guha, R. Weber, A. H. Goldstein, and R. C. Cohen.
 436 On the temperature dependence of organic reactivity, nitrogen oxides, ozone production, and
 437 the impact of emission controls in San Joaquin Valley, California. *Atmospheric Chemistry and*
 438 *Physics*, 14(7):3373–3395, 2014.

439 S. E. Pusede, A. L. Steiner, and R. C. Cohen. Temperature and Recent Trends in the Chemistry
 440 of Continental Surface Ozone. *Chemical Reviews*, 115(10):3898–3918, 2015.

441 D. J. Rasmussen, J. Hu, A. Mahmud, and M. J. Kleeman. The ozone–climate penalty: Past,
 442 present, and future. *Environmental Science & Technology*, 47(24):14258–14266, 2013. PMID:
 443 24187951.

444 A. Rickard, J. Young, M. J. Pilling, M. E. Jenkin, S. Pascoe, and S. M. Saunders. The Master
 445 Chemical Mechanism Version MCM v3.2. <http://mcm.leeds.ac.uk/MCMv3.2/>, 2015. [Online;
 446 accessed 25-March-2015].

447 J. I. Rubin, A. J. Kean, R. A. Harley, D. B. Millet, and A. H. Goldstein. Temperature dependence
 448 of volatile organic compound evaporative emissions from motor vehicles. *Journal of Geophysical*
 449 *Research: Atmospheres*, 111(D3), 2006. D03305.

450 Y. Sadanaga, A. Yoshino, S. Kato, , and Y. Kajii. Measurements of oh reactivity and
 451 photochemical ozone production in the urban atmosphere. *Environmental Science & Technology*,
 452 39(22):8847–8852, 2005. PMID: 16323785.

453 R. Sander, A. Kerkweg, P. Jöckel, and J. Lelieveld. Technical note: The new comprehensive
 454 atmospheric chemistry module mecca. *Atmospheric Chemistry and Physics*, 5(2):445–450, 2005.

455 S. M. Saunders, M. E. Jenkin, R. G. Derwent, and M. J. Pilling. Protocol for the development of
 456 the Master Chemical Mechanism, MCM v3 (Part A): tropospheric degradation of non-aromatic
 457 volatile organic compounds. *Atmospheric Chemistry and Physics*, 3(1):161–180, 2003.

458 J. L. Schnell, M. J. Prather, B. Josse, V. Naik, L. W. Horowitz, P. Cameron-Smith, D. Bergmann,
 459 G. Zeng, D. A. Plummer, K. Sudo, T. Nagashima, D. T. Shindell, G. Faluvegi, and S. A. Strode.
 460 Use of north american and european air quality networks to evaluate global chemistry–climate
 461 modeling of surface ozone. *Atmospheric Chemistry and Physics*, 15(18):10581–10596, 2015.

462 S. Sillman. The use of NO_y, H₂O₂, and HNO₃ as indicators for ozone-NO_x-hydrocarbon sensitivity
 463 in urban locations. *Journal of Geophysical Research: Atmospheres*, 100(D7):14175–14188, 1995.

464 S. Sillman. The relation between ozone, NO_x and hydrocarbons in urban and polluted rural
 465 environments. *Atmospheric Environment*, 33(12):1821 – 1845, 1999.

466 S. Sillman and P. J. Samson. Impact of temperature on oxidant photochemistry in urban,
 467 polluted rural and remote environments. *Journal of Geophysical Research: Atmospheres*, 100
 468 (D6):11497–11508, 1995.

469 D. Simpson, A. Benedictow, H. Berge, R. Bergström, L. D. Emberson, H. Fagerli, C. R. Flechard,
 470 G. D. Hayman, M. Gauss, J. E. Jonson, M. E. Jenkin, A. Nyíri, C. Richter, V. S. Semeena,
 471 S. Tsyro, J.-P. Tuovinen, Á. Valdebenito, and P. Wind. The EMEP MSC-W chemical transport
 472 model – technical description. *Atmospheric Chemistry and Physics*, 12(16):7825–7865, 2012.

473 A. L. Steiner, S. Tonse, R. C. Cohen, A. H. Goldstein, and R. A. Harley. Influence of future
 474 climate and emissions on regional air quality in California. *Journal of Geophysical Research:*
 475 *Atmospheres*, 111(D18), 2006. D18303.

476 W. R. Stockwell, P. Middleton, J. S. Chang, and X. Tang. The second generation regional acid
 477 deposition model chemical mechanism for regional air quality modeling. *Journal of Geophysical*
 478 *Research: Atmospheres*, 95(D10):16343–16367, 1990.

479 W. R. Stockwell, F. Kirchner, M. Kuhn, and S. Seefeld. A new mechanism for regional atmospheric
 480 chemistry modeling. *Journal of Geophysical Research: Atmospheres*, 102(D22):25847–25879,
 481 1997.

482 E. von Schneidemesser, P. S. Monks, J. D. Allan, L. Bruhwiler, P. Forster, D. Fowler, A. Lauer,

483 W. T. Morgan, P. Paasonen, M. Righi, K. Sindelarova, and M. A. Sutton. Chemistry and the
484 Linkages between Air Quality and Climate Change. *Chemical Reviews*, 2015. PMID: 25926133.

485 E. von Schneidemesser, J. Coates, A. J. H. Visschedijk, H. A. C. Denier van der Gon, and T. M.
486 Butler. Variation of the NMVOC speciation in the solvent sector and the sensitivity of modelled
487 tropospheric ozone. *Atmospheric Environment*, Submitted for Publication, 2016.

488 P. Wagner and W. Kuttler. Biogenic and anthropogenic isoprene in the near-surface urban
489 atmosphere — A case study in Essen, Germany. *Science of The Total Environment*, 475:104 –
490 115, 2014.

491 G. Yarwood, S. Rao, M. Yocke, and G. Z. Whitten. Updates to the Carbon Bond Chemical
492 Mechanism: CB05. Technical report, U. S Environmental Protection Agency, 2005.